1

Detection of chirality and mutations of knots and links

RAMADEVI PICHAI

*Department of Physics, Indian Institute of Technology Bombay,
Mumbai,Maharashtra-400 076, INDIA*
*E-mail: ramadevi@phy.iitb.ac.in

In this brief presentation, we would like to present our attempts of detecting chirality and mutations from Chern-Simons gauge theory. The results show that the generalised knot invariants, obtained from Chern-Simons gauge theory, are more powerful than Jones, HOMFLYPT and Kauffman polynomials. However the classification problem of knots and links is still an open challenging problem.

Keywords: chirality, mutation, Chern-Simons field theory invariants

1. Introduction

The classification of three and four manifolds is one of the open questions which has been addressed by both mathematicians and physicists. In particular, physicists have shown that a class of quantum field theories called topological field theories provides an elegant approach to solve these problems.

The main idea in any quantum field theory is to represent the theory by an action S which gives information about the particle content and their interactions. The interaction strengths are given by coupling constants. For capturing the topological features of knots or links as shown in Fig. 1, we need a theory which does not change if we alter the shape or size of these knots or links. One such theory is the Chern-Simons gauge theory where the action S is explicitly metric independent. Hence, Chern-Simons field theory provides a natural framework to study knots,links and three manifolds. The action S defining the Chern-Simons theory on a three manifold M based
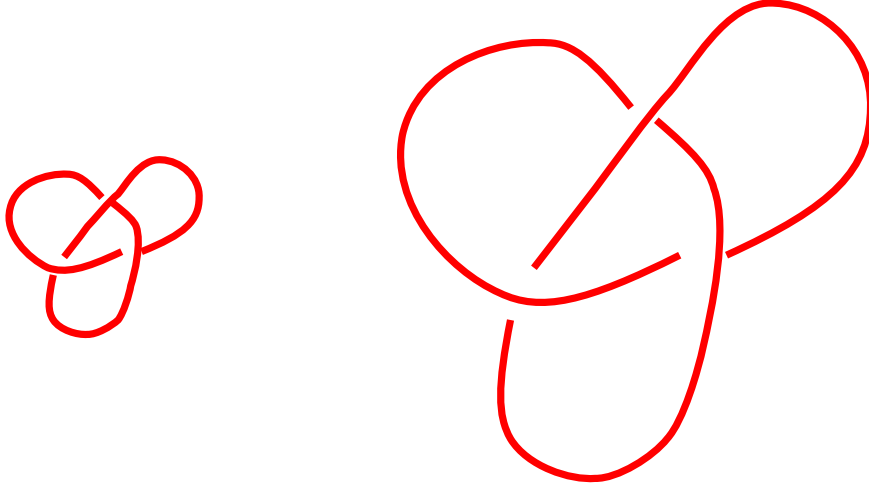
2

Fig. 1.   Both knots C (though different sizes) are trefoil knots

on a gauge group G is

$$
\begin{aligned}
S &= \frac{k}{4\pi} \int_M Tr \left(A \wedge dA + \frac{2}{3} A \wedge A \wedge A \right) \\
&= \frac{k}{4\pi} \int_M \epsilon_{\mu\nu\lambda} \, d^3x \, Tr \left(A_\mu \partial_\nu A_\lambda + \frac{2}{3} A_\mu A_\nu A_\lambda \right) ,
\end{aligned}
\tag{1}
$$

where k is the coupling constant and A_μ's are the gauge fields or connections matrix-valued in group G.

The knots or links - for example, the trefoil knot C carrying representation R of the gauge group G are described by the expectation value of Wilson loop operators $W_R(C) = Tr[Pexp \oint A_\mu dx^\mu]$:

$$
V_R[C] = \langle W_R(C) \rangle \;\; = \;\; \frac{\int_M [\mathcal{D}A] \, W_R(C) \, exp(iS)}{\mathcal{Z}[M]} \; ,
\tag{2}
$$

where

$$
\mathcal{Z}[M] = \int_M [\mathcal{D}A] \, exp(iS)
$$

is the partition function and $V_R[C]$ are the knot invariants.

Witten's pioneering work[1] established a three-dimensional definition for knots and links. In particular, Jones and HOMFLYPT polynomials and their recursion relations were obtained from Chern-Simons gauge theory

based on $SU(2)$ and $SU(N)$ gauge groups. We can relate coupling constant k and the rank N to the polynomial variables of HOMFLYPT polynomials. Similarly, the Jones' polynomial variable q will be related as $q = \exp(2\pi i/k + 2)$.

The two main ingredients which go into the evaluation of the polynomial invariants $V_R[C]$ of knots and links are

(1) Connection between Chern-Simons theory on the three-dimensional ball to the two-dimensional Wess-Zumino conformal field theory on the boundary of the three-ball.

(2) Using Alexander's theorem, any knot or link can be obtained as a closure of braid.

In Fig. 2(a), we illustrate Alexander's theorem by re-drawing the trefoil knot as a closure of two-strand braid with three crossings. Also, we have diagrammatically shown in Fig. 2(b) that these knots or links in S^3 can be viewed as gluing two three-balls with oppositely oriented S^2 boundaries. In this particular trefoil knot example, the S^2 boundary has four-punctures. The connection between Chern-Simons theory and Wess-Zumino conformal field theory states that the Chern-Simons functional integral over a three-ball with a four-punctured S^2 boundary corresponds to state $|\Psi_3\rangle$ which represents four-point correlator conformal block in the Wess-Zumino conformal field theory. The suffix 3 on the state is to indicate that the middle two-strands are braided thrice. In fact, the punctures get exchanged whenever the middle two-strands get braided. We can denote the no-crossing four-punctured boundary state as $|\Psi_0\rangle$ and apply a braiding operator $\mathcal{B}$ thrice to get the state $|\Psi_3\rangle$:

$$|\Psi_3\rangle = \mathcal{B}^3|\Psi_0\rangle \ . \tag{3}$$

Similarly, the state for the oppositely oriented boundary will be in the dual space. For the above example in Fig. 2(b), the state is $\langle\Psi_0|$. The knot invariant is

$$V_R[C] = \langle\Psi_0|\Psi_3\rangle = \langle\Psi_0|\mathcal{B}^3|\Psi_0\rangle \ . \tag{4}$$

In order to see the polynomial form, we need to expand the state $|\Psi_0\rangle$ in an eigenbasis of the braiding operator $\mathcal{B}$. In general for the four-punctured S^2 boundary, the braiding can be either on the side two-strands or on the middle two strands. For clarity, we will take the gauge group $G = SU(2)$. For the four-punctured S^2 boundary, we can chose eigenbasis $|\phi_s\rangle$ if the
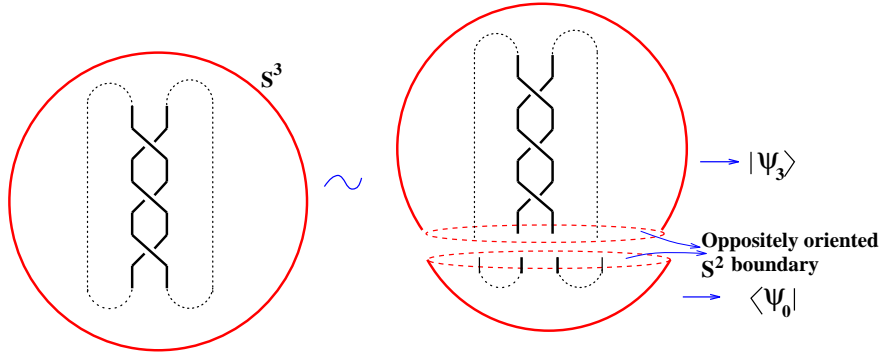
4

Fig. 2.   (a) Trefoil in S^3 drawn as a closure of braid $\equiv$ (b) gluing of two three-balls with oppositely oriented S^2 boundaries
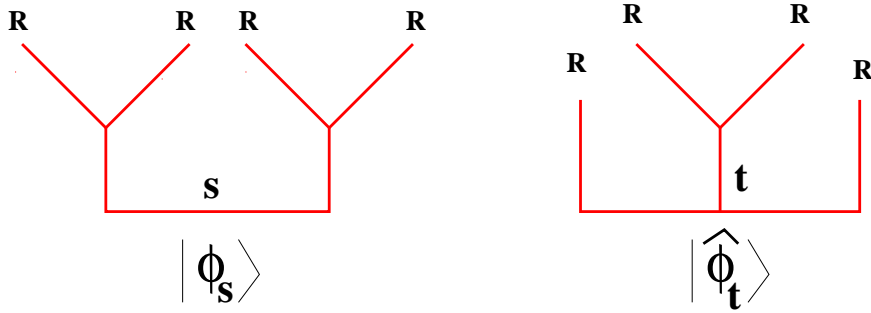

Fig. 3.   eigenbasis when braiding (a) side two-strands (b) middle two-strands.

braiding is in the side two-strands. That is,

$$\mathcal{B}_1|\phi_s\rangle = \lambda_s(R,R)|\phi_s\rangle \ , \tag{5}$$

where the suffix 1 on the braiding operator denotes the braiding between first and the second strands and the eigenvalue is $\lambda_s(R,R)$. The basis is shown diagrammatically in Fig. 3(a) where R denotes the $SU(2)$ representation placed on the strands. From the picture, the representation s will be an element in the tensor product $R \otimes R$. Similarly, for braiding middle two strands, we choose the basis $|\hat{\phi}_t\rangle$ as shown in Fig. 3(b) where $t \in R \otimes R$. Clearly, these two basis states must be related by a duality matrix:

$$|\hat{\phi}_t\rangle = a_{ts}\begin{bmatrix} R\ R \\ R\ R \end{bmatrix}|\phi_s\rangle \ . \tag{6}$$

When the four strands carry the same representation, we can write in short-

hand notation the duality matrix as

$$a_{ts} \begin{bmatrix} R \ R \\ R \ R \end{bmatrix} \equiv a_{ts} \ . \tag{7}$$

These duality matrices turns out to be proportional to quantum Racah coefficients. The explicit form of $SU(2)_q$ Racah coefficients and their identities satisfied are available in Ref. 2. See also papers[3–5] . In this example, the braiding involves middle two strands. Hence the state $|\Psi_0\rangle$ can be expanded in the middle-strand basis $|\hat{\Phi}_t\rangle$:

$$|\Psi_0\rangle \ = \ \sum_t \mu_t \ |\hat{\Phi}_t\rangle \ . \tag{8}$$

Interestingly, the coefficients μ_t has to satisfy

$$\mu_t \ = \ \sqrt{V_t[U]} \ = \ \sqrt{S_{0t}/S_{00}} \equiv \sqrt{dim_q t} \ , \tag{9}$$

so that two equivalent knots share the same polynomial invariant. Here, $V_t[U]$ denotes the polynomial invariant for unknot carrying representation t whose form can be written as the ratio of elements of the modular transformation matrix S in Wess-Zumino conformal field theory or in terms of quantum dimensions of the representation t of the quantum group as indicated in the above equation. The knot invariant (4) will be

$$V_R[C] \ = \ \langle\Psi_0|\mathcal{B}^3|\Psi_0\rangle \ = \ \sum_t dim_q t(\lambda_t(R,R))^3 \ . \tag{10}$$

So far, we have not introduced orientation on the strands. In general, the braiding eigenvalue depends on the **framing** and also on the relative orientation on the two braiding strands. Two conventional framing are standard framing and blackboard framing. Standard framing is one where the self-linking number of the knot with its frame is zero. This is useful to obtain ambient isotopy invariants. The self-linking number matches the crossing number in the blackboard framing. Hence the braiding eigenvalue in the blackboard framing is useful to obtain regular isotopy invariants. In the trefoil example, we could place parallel orientation in the middle two-strands. As the crossing sign due to braiding is positive, we called such a braiding as right-handed braiding. Similarly, an inverse braiding leading to mirror of trefoil (T^*) will be called left-handed braiding.

For parallely oriented strands, the right-handed braiding eigenvalue in standard framing is

$$\lambda_t^{(+)}(R,R) \ = \ (-1)^\epsilon q^{2C_R - C_t/2}, \ q = e^{\frac{2\pi i}{k+C_v}}. \tag{11}$$

6

where C_R, C_t, C_v denotes the quadratic casimirs in the respective R, t and adjoint representation. ϵ will be ± 1 depending on the representation t appears symmetrically or antisymmetrically in the tensor product $R \otimes R$. Similarly, the left-handed braiding eigenvalue for antiparallely oriented strands is

$$\lambda_t^{(-)}(R,R) \;=\; (-1)^\epsilon q^{C_t/2}, \; q = e^{\frac{2\pi i}{k+C_v}}. \tag{12}$$

Now using the appropriate braiding eigenvalues, the knot invariants can be written as polynomials in the variable q. The method for a four-punctured S^2 boundary is generalisable for r such four-punctured S^2 boundaries as shown in Fig. 4. We will see in the next section that this building block will be useful to redraw knots like knot 9_{42} and knot 10_{71} as gluing of three-balls with one or more four-punctured S^2 boundaries. The basis state for such a r-S^2 boundaries is

$$\nu_r \;=\; \sum_{R_s} \frac{|\phi_{R_s}^{(1)side}\rangle |\phi_{R_s}^{(2)side}\rangle \cdots |\phi_{R_s}^{(r)side}\rangle}{(dim_q R_s)^{\frac{r-2}{2}}} \;, \tag{13}$$

where $R_s \in R_i \otimes R_{i+1}$ for any i. Sometimes, it is useful to keep S^2 boundaries with more than four-puctures. Then the basis state for a S^2 boundary with n puctures will be a n-point conformal block. For braiding $\mathcal{B}_{2i+1}$'s and $\mathcal{B}_{2i}$'s, we choose the basis shown in Fig. 5(a) and (b) respectively. The procedure we elaborated for the trefoil obtained from gluing two three-balls each with a four-punctured S^2 boundary is generalisable for any knot. That is, using the building blocks in Fig. 4 or three-balls with n-punctured S^2 boundaries, it is not difficult to see that any knot can be obtained either from gluing two three-balls each with a n-punctured S^2 boundaries or from gluing many three-balls with one or more r four-puctured S^2 boundaries. The method presented here enables direct evaluation of any knot/link polynomial directly without going through the recursive procedure.

Though we have concentrated on the gauge group $SU(2)$, it is straightforward to generalise for any compact semi-simple gauge group.[6] The representation R must be replaced by conjugate representation $\bar{R}$ ($R \equiv \bar{R}$ for $SU(2)$) depending on the oriented strand is outgoing from or incoming to a S^2 boundary as shown in Fig. 4. Thus, we can place any representation R of any compact semi-simple gauge group on the knot and obtain **generalised knot invariants.** If we place the defining representation on the strands, we recover some of the well-known polynomials as tabulated below:
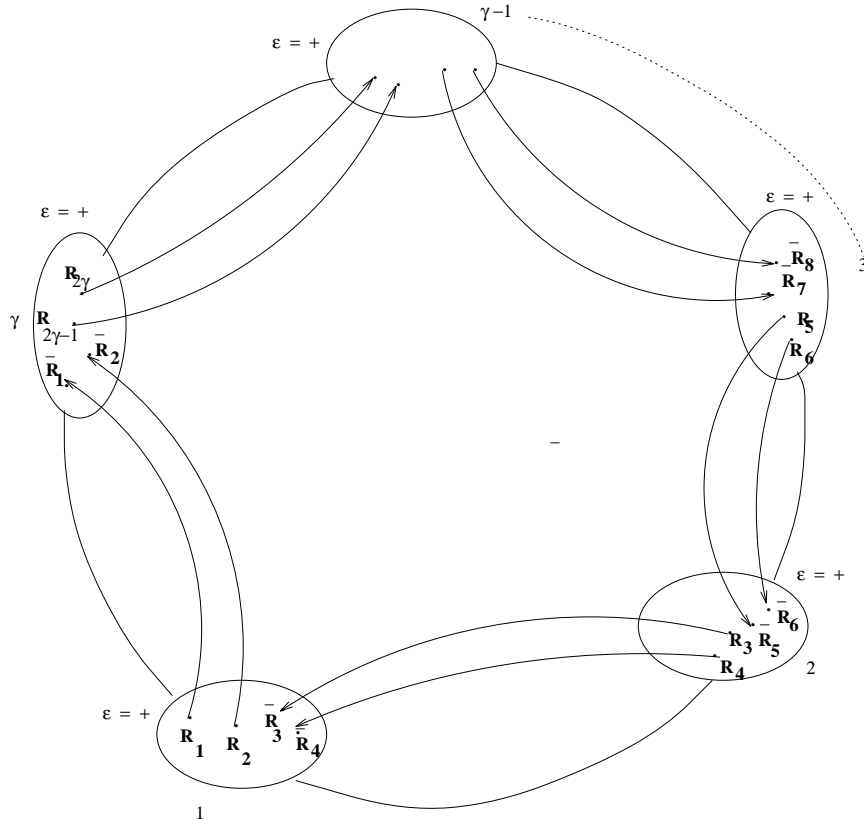
Fig. 4.   Three-ball with r S^2 boundaries each with four-punctures.

Gauge Group	Polynomial
$SU(2)$	Jones'
$SU(N)$	Two-variable HOMFLYPT
$SO(N)$	Two-variable Kauffman

We know that these well-known polynomials do not solve the classification problem. Apart from these special cases, Chern-Simons field theory gives a huge pool of generalised polynomials depending on placing representation R of any gauge group other than the defining representation on the strands. We believe that at least one of these generalised Chern-Simons invariant will be able to distinguish two inequivalent knots which are not distinguished by the well-known polynomials.

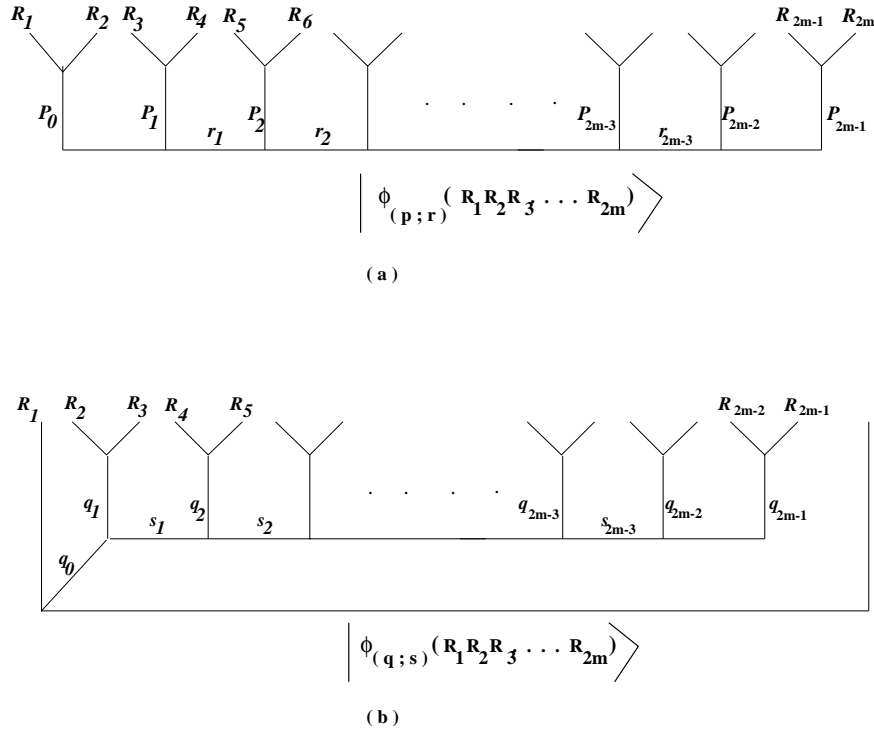Knot theory literature gives a list of chiral knots and mutant knots

8

Fig. 5.   Basis states for a n-punctured S^2 boundary.

which are not distinguished by Jones', HOMFLYPT and Kauffman. We tried to check the ability of generalised knot invariants, from Chern-Simons field theory, to detect **chirality and mutations**. We address the chirality detection in the following section.

2. Chirality Detection

Upto 10 crossings, there are two knots : knot 9_{42} and knot 10_{71} which are chiral but their chirality is not detected by the well-known polynomials. In Fig. 6, we have drawn **knot** 9_{42} in two equivalent ways. Clearly, the knot 9_{42} can be obtained as gluing of five building blocks as shown in Fig. 7.

For $G = SU(2)$, $R_n = \overset{\longleftarrow n \longrightarrow}{\boxed{}}$ (spin $n/2$ representation) placed on knot, the states for the building blocks can be written down following the methods presented in the previous section and also using the properties of the duality matrix.[3–5] The states for these five building blocks are[7]
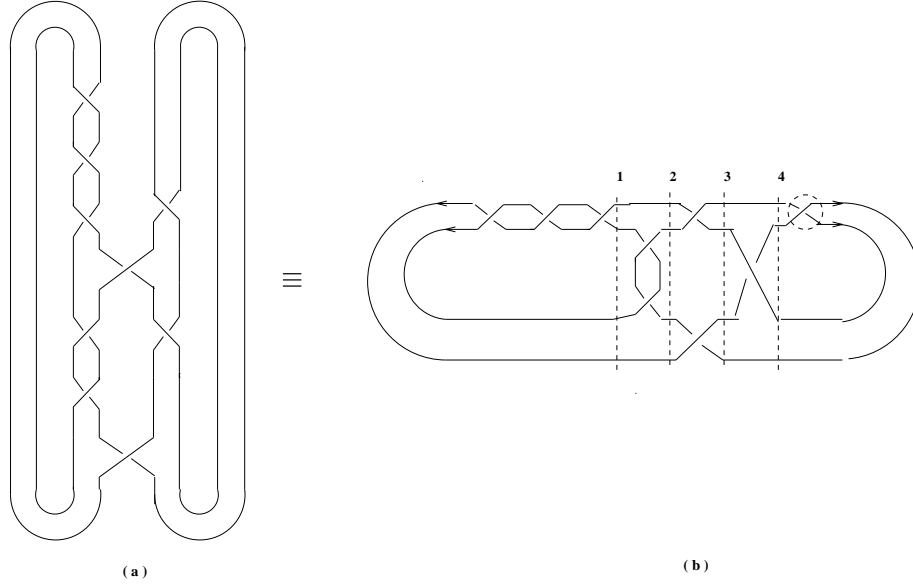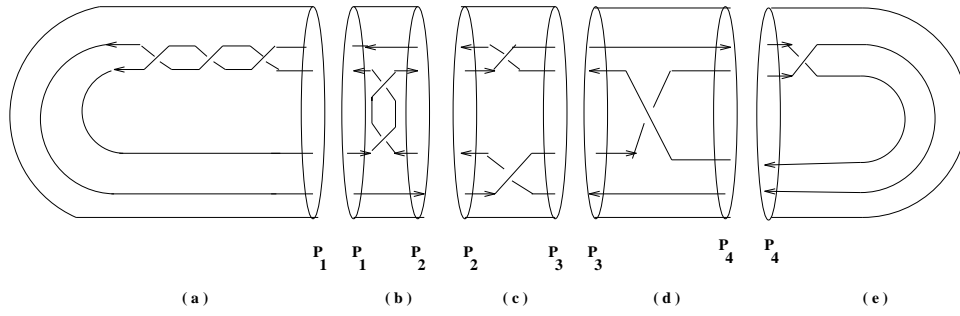
Fig. 6.   Chiral Knot 9_{42}

Fig. 7.   Gluing of five building blocks

$$\nu_1(P_1) = \sum_{l_1=0}^{n} \sqrt{[2l+1]}(-1)^{3(n-l_1)} q^{-3/2[n(n+2)-l_1(l_1+1)]} |\phi_{l_1}^{(1)}\rangle$$

$$\nu_1(P_4) = \sum_{l_5=0}^{n} (-1)^{n-l_5} q^{-1/2[n(n+2)-l_5(l_5+1)]} |\phi_{l_5}^{(1)}\rangle$$

$$\nu_2(P_1; P_2) = \sum_{i_1,j_1,l_2,r=0}^{n} \frac{a_{l_1 r} a_{j_1 r} a_{l_2 r} \sqrt{[2l_2+1]}}{\sqrt{[2r+1]}} \times q^{n(n+2)-l_2(l_2+1)} |\phi_{i_1}^{(1)}\rangle |\phi_{j_1}^{(2)}\rangle$$

$$\nu_2(P_2; P_3) = \sum_{l_3=0}^{n} q^{l_3(l_3+1)} |\phi_{l_3}^{(1)}\rangle |\phi_{l_3}^{(2)}\rangle$$

$$\nu_2(P_3; P_4) = \sum_{i_2,j_2,l_4=0}^{n} (-1)^{l_4} q^{-l_4(l_4+1)/2} a_{l_4 i_2} a_{l_4 j_2} |\phi_{i_2}^{(1)}\rangle |\phi_{j_2}^{(2)}\rangle \; .$$

10

Here P_i's denote the S^2 boundaries as indicated in Fig. abg:fig7. Using the above states, the knot invariant is

$$V_n[9_{42}] = (-1)^n q^{\frac{-3}{2}[n(n+2)]} \sum_{r,l_1,l_2,j_1,j_2=0} \sqrt{[2l_1+1]} \times$$
$$\sqrt{[2l_2+1]}\sqrt{[2j_2+1]} a_{l_1 r} a_{l_2 r} a_{j_1 r} a_{j_1 j_2} \times$$
$$(-1)^{l_1} q^{\frac{3}{2}[l_1(l_1+1)]} q^{\frac{3}{2}[j_1(j_1+1)]} q^{-l_2(l_2+1)} q^{j_2(j_2+1)}$$

We checked the general result for the special cases. That is, $n = 1$ gives Jones' polynomial and $n = 2$ gives Akutsu-Wadati/Kauffman polynomial.[8] Interestingly, for $n = 3$, the polynomial is

$$\begin{aligned}
V_3[9_{42}] = \; & q^{45/2} - q^{41/2} - q^{39/2} + q^{35/2} + q^{23/2} + q^{21/2} - q^{19/2} \\
& -q^{17/2} + q^{13/2} - q^{9/2} + q^{5/2} + q^{3/2} + q^{-3/2} + q^{-5/2} \\
& -q^{-13/2} - q^{-15/2} + q^{-21/2} + 2q^{-23/2} - q^{-27/2} + 2q^{-31/2} \\
& -3q^{-35/2} - q^{-37/2} + q^{-39/2} + q^{-41/2} \; .
\end{aligned}$$

Clearly, $V_3[9_{42}](q) \neq V_3[9_{42}](q^{-1})$ indicating that $SU(2)$ Chern-Simons spin $3/2$ ($n = 3$ in representation R_n) knot polynomial is powerful to detect chirality. Similar exercise was performed for knot 10_{71} by gluing the four building blocks as shown in Fig. 8. The knot invariant[7] is

$$V_n[10_{71}] = (-1)^n q^{\frac{n(n+2)}{2}} \sum_{i,r,s,u,m=0} \sqrt{\frac{[2r+1][2s+1][2u+1]}{[2m+1]}} a_{im}$$
$$a_{ms} a_{rm} a_{iu} (-1)^s \; q^{-i(i+1)} q^{m(m+1)} q^{-r(r+1)} q^{u(u+1)} q^{\frac{3}{2}s(s+1)} \; .$$

For $n = 3$, we have checked that $V_3[10_{71}](q) \neq V_3[10_{71}](q^{-1})$ confirming the ability of generalised Chern-Simons invariant in detecting chirality. With such positive results for chiral knots, we attempted to check whether generalised Chern-Simons invariant is capable of detecting mutation operation which we shall present in the following section.

3. Mutation and mutant knots

Remove a two-tangle region from any knot and do a rotation by π about any of the three perpendicular axis. Replace the rotated two-tangle back with suitable reversal of orientation of the strands to give another knot. This operation is called mutation and the two knots are said to be mutants. In Fig. 9, we have indicated the three mutation operation γ_i's. An example for the mutant knots is the well-known eleven-crossing Kinoshita-Terasaka and Conway knots. We can formally represent mutant knots shown in Fig. 10 as
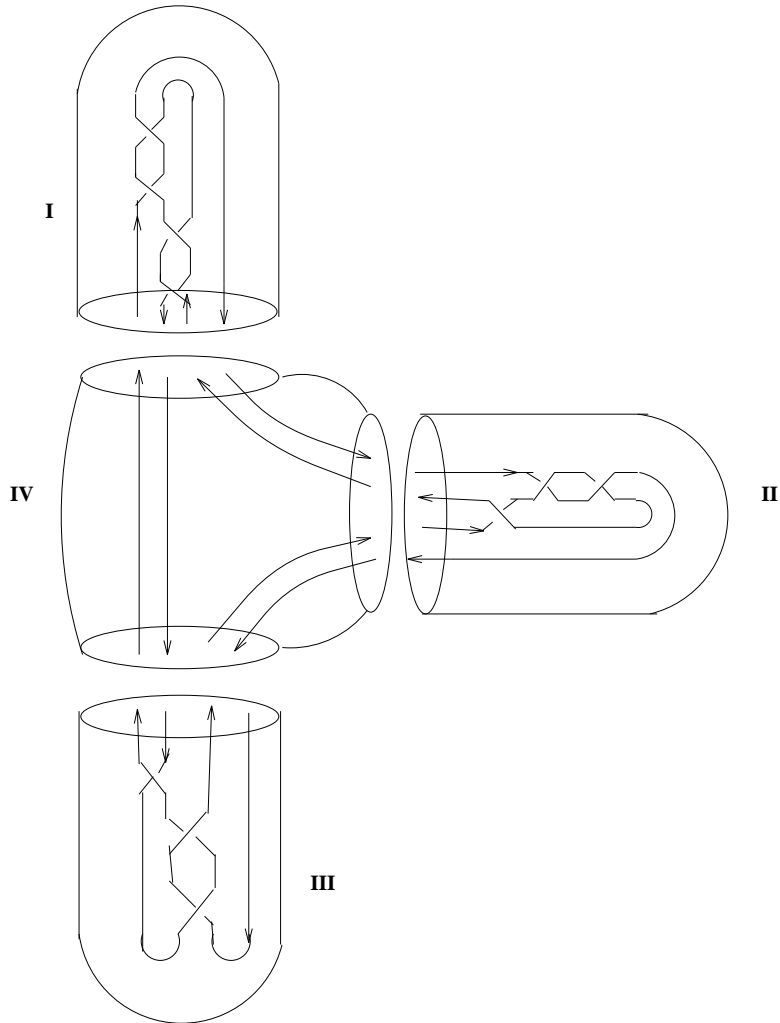
Fig. 8.   Chiral Knot 10_{71} obtained from gluing the building blocks

gluing two three-balls with the two-tangle rooms as shown in Fig. 11. That is, gluing Fig. 11(d) with any of the Fig. 11(a),(b) and (c) gives mutant knots. Interestingly, the states (a), (b), (c) in Fig. 11 can be obtained by gluing Fig. 11(a) with the two-boundary states (a), (b) and (c) in Fig. 12 respectively. Clearly, ν_2 and ν_3 represent mutation γ_1 and γ_2 respectively in Fig. 9 respectively. As braid words, Fig. 12 (a), (b), (c) are different but
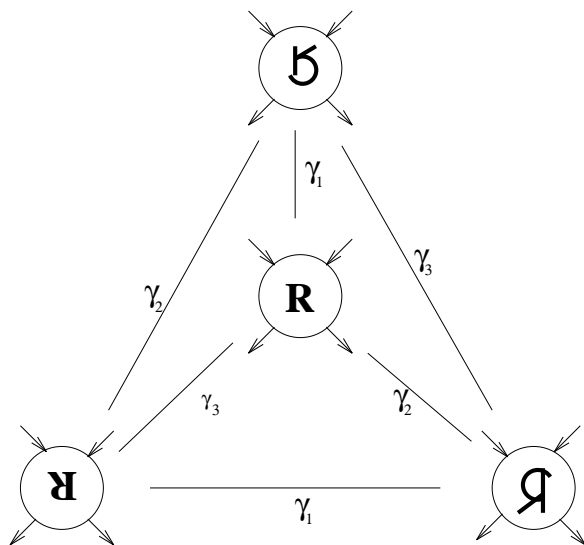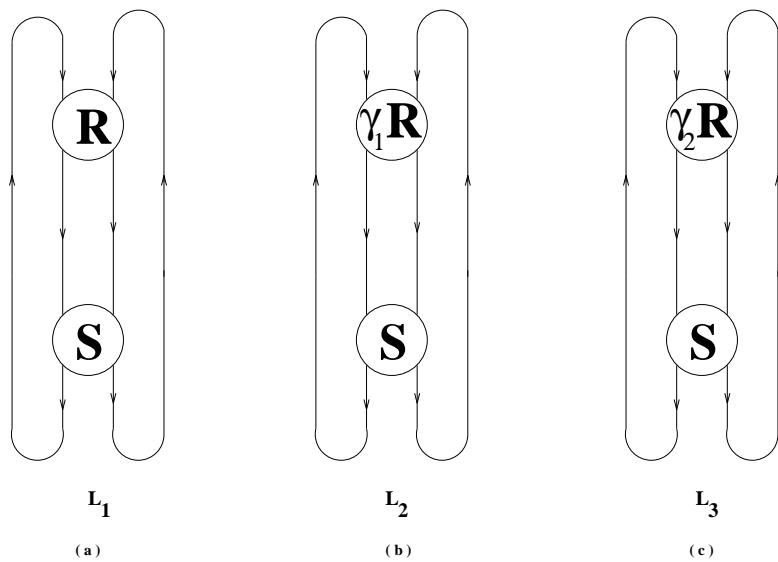
12

Fig. 9.   Mutation Operation

Fig. 10.   Mutant Knots

the states ν_i's are same:

$$\nu_2 = \sum_l |\phi_l^{side(1)}\rangle b_1 b_3^{-1} |\phi_l^{side(2)}\rangle = \mathcal{C}\nu_1 . \tag{14}$$
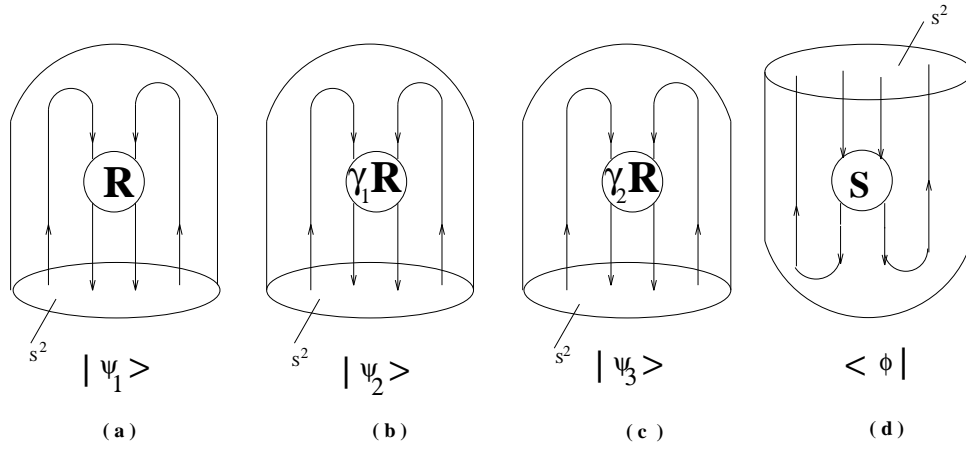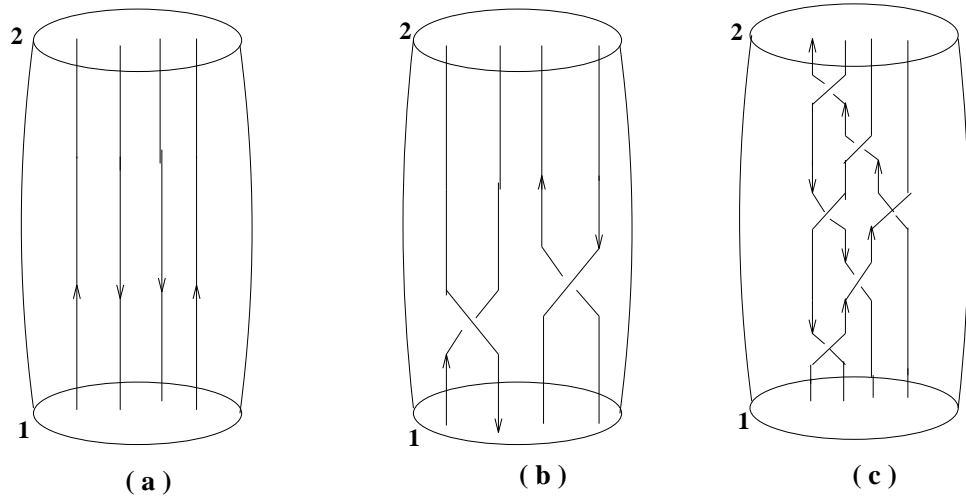
Fig. 11.   Building blocks

Fig. 12.   state (a) ν_1 (b) ν_2 and (c) ν_3 .

where we have used

$$b_1|\phi_l^{side}\rangle = b_3|\phi_l^{side}\rangle = \lambda_l^{(-)}(R, \bar{R})|\phi_l^{side}\rangle \ ,$$

and the operator $\mathcal{C}$ interchanges the representations on the first and second, the third and fourth punctures in that basis. Similarly, we can show

$$\nu_3 \ = \ \sum_l |\phi_l^{side(1)}\rangle b_1 b_2 b_1 b_3 b_2 b_1 |\phi_l^{side(2)}\rangle = \mathcal{C}\nu_1 \ . \tag{15}$$

14

So, the **generalised invariants** of the mutants L_1, L_2, L_3 obtained by gluing Fig. 11(a),(b) and (c) with (d) are **same**.

It appears that the identities of the states for **four-punctured boundaries** play a crucial role in making the states representing the mutation operation (ν_2, ν_3) to be similar to identity braid ν_1. In order to go beyond four-punctured boundary state, we studied composite braiding[9] . Using the representation theory of composite braids, we showed that the composite invariant for knots are sum of the generalised knot invariants. This implies composite invariants cannot detect mutations in knots. However, some mutant links can be distinguished by composite invariants.

4. Summary and Discussion

In this article, we have briefly presented the direct evaluation of generalised invariants of knots and links from Chern-Simons field theory. For $SU(2)$ gauge group in Chern-Simons theory, we get the the colored Jones' polynomials for the knots and links carrying higher dimensional $SU(2)$ representations. There is a huge pool of generalised Chern-Simons invariants for other gauge groups like $SU(N)$, $SO(N)$ etc with knots and links carrying arbitrary representations. The hope is that at least one of the invariants will be able to distinguish two inequivalent knots.

We showed that the chiral knots upto 10 crossings are distinguished by the Chern-Simons field theory invariants. However, we gave a proof that the process of mutation cannot be detected within the Chern-Simons field theoretic framework. The proof is for knots and links carrying arbitrary representation of any compact semi-simple gauge group.

Discussions during the knot theory conference revealed that there are approaches from quantum groups[10] and Floer homology[11] whose invariants does distinguish 11-crossing Kinoshita-Terasaka and Conway mutant knot. It will be interesting to to check whether this method distinguishes other mutant knots.

References

1. E. Witten, Commun. Math. Phys. **121** (1989) 351.
2. A.N. Kirillov, N.Yu. Reshetikhin, *Representation algebra $U_q(sl_2)$, q-orthogonal polynomials and invariants of links*, LOMI preprint E-9-88; see also in: New Developments in the Theory of Knots. ed. T. Kohno, World Scientific (Singapore, 1989).
3. R.K. Kaul and T.R. Govindarajan, Nucl. Phys. **B380** (1992) 293.
4. R.K. Kaul and T.R. Govindarajan, Nucl. Phys. **B393** (1993) 392.

5. R.K. Kaul, Commun. Math. Phys.**162** (1994) 289.
6. P. Ramadevi, T.R. Govindarajan and R.K. Kaul, Nucl. Phys. **B402** (1993) 548
7. P. Ramadevi, T.R. Govindarajan and R.K. Kaul, Mod. Phys. Lett **A9** (1994) 3205.
8. M.Wadati, T.Deguchi and Y.Akutsu, Phys. Rep. **180** (1989) 247 and references therein.
9. P. Ramadevi, T.R. Govindarajan and R.K. Kaul, Mod. Phys. Lett **A10** (1995) 1635.
10. H.R.Morton and H.J.Ryder, Geom. Topol. Monogr.**1** (1998)365.
11. John A. Baldwin, W.D.Gilam, *Computations of Heegard-Floer knot homology*, arXiv:math/0610167.